Lithos 246–247 (2016) 99–109

Contents lists available at ScienceDirect

Lithos

journal homepage: www.elsevier.com/locate/lithos

Syn-collisional granitoids in the Qilian Block on the Northern Tibetan Plateau: A long-lasting magmatism since continental collision through slab steepening

Hui Huang [a,*], Yaoling Niu [a,b,c,*], Xuanxue Mo [a]

[a] School of Earth Science and Mineral Resources, China University of Geosciences, Beijing 100083, China
[b] Department of Earth Sciences, Durham University, Durham DH1 3LE, UK
[c] Institute of Oceanology, Chinese Academy of Sciences, Qingdao 266071, China

ARTICLE INFO

Article history:
Received 22 April 2015
Accepted 17 December 2015
Available online 5 January 2016

Keywords:
Long-lasting magmatism
Syn-collisional granitoids
Slab break-off
Slab steepening
Qilian Orogenic Belt
Qilian Block

ABSTRACT

In this paper we present a new model that can explain the large zircon age spectrum of ~510 – 420 Ma within a single sample from the Gangcha (Gcha) biotite granodiorite and the Huangyuan (HY) two-mica monzogranite on the northern Tibetan Plateau. The large age spread recorded in zircons is characteristic of granitoid samples from the studied region, which is best explained by the long-lasting magmatism since the onset of continental collision at ~500 Ma, followed by slab steepening and the ultimate slab break-off at ~450 Ma. These granitoids have a large major and trace element compositional variation, but limited initial Sr ($I_{Sr[450]} = 0.709$ to 0.715), Nd ($_{Nd[450]} = -6.5$ to -3.7), Hf ($_{Hf[450]} = -4.3$ to 1.5) and Pb ($^{206}Pb/^{204}Pb_{[450]} = 17.70$ to 17.17; $^{207}Pb/^{204}Pb_{[450]} = 15.60$ to 15.69; $^{208}Pb/^{204}Pb_{[450]} = 38.04$ to 38.73) isotopic variation. The small negative whole rock $_{Nd[450]}$ and $_{Hf[450]}$ values are most consistent with the granitoid source being dominated by subducted seafloor materials. The inherited zircons with large negative $_{Hf[450]}$ values (e.g. -50) are indicative of input from the lower continental crust and subducted sediments. The correlated variations among major elements, trace elements and radiogenic isotopes are best interpreted as reflecting melting-induced mixing of a compositionally heterogeneous source with superimposed effect of varying extent of fractional crystallization and crustal assimilation. The inherited zircons of Palaeo-Proterozoic age and the Archean crustal model ages signify the involvement of ancient basement rocks.

1. Introduction

Granitoids provide indispensable information for the reconstruction of the history of orogenic belts. Their age relationships to the adjacent tectonic units provide strong constraints for the temporal and tectonothermal evolution of the entire orogenic belt. The Qilian Orogenic Belt (QOB) on the northern margin of the Greater Tibetan Plateau records the complete histories of continental breakup, seafloor spreading, ocean basin closing and the ultimate continental collision from the Neoproterozoic to the Paleozoic (Fig. 1; Song, et al., 2013, 2014 and references therein). The subunit Qilian Block (QB) lies between the North Qilian Orogenic Belt (NQOB) consisting of a subduction complex and the North Qaidam-ultrahigh pressure metamorphic belt (NQ-UHPM) (Fig. 1, Song, et al., 2013, 2014 and references therein). Despite the relatively detailed studies on the metamorphic rocks and the increasing knowledge of the magmatic rocks in the NQOB and NQ-UHPM, some key questions remain poorly addressed. These include the timing of collision and relationship between different subunits (Xu et al., 1994, 2006; Yin and Harrison, 2000; Yang et al., 2002, 2006; Gehrels et al., 2003, 2011; Song et al., 2006, 2013, 2014; Wu et al., 2006a, 2010; Xiao et al., 2009; Huang et al., 2015).

The solution to the above debate lies in better understanding the nature and histories of the QB (Fig. 1). A recent study found that plutons in the QB of syn-collisional origin have a large compositional variation and large zircon age spread within individual samples (Huang, et al., 2015). This age spectra cannot be divided into groups due to their indistinguishable zircon cathodoluminescence (CL) images and compositions, and its origin remains unclear. We note that the similarly large age spread within a single sample exists not only in the QB granitoids, but has also been observed in granitoids and metamorphic rocks in the NQ-UHPM. Crustal partial melting can last a long duration up to 30 million years (Sawyer et al., 2011). In central Iberia, continuous anatexis lasted for 55 million years since continental collision (Montero et al., 2004). While in the eastern Swiss Alps and north Dabie Terrane, records in meta-igneous rocks demonstrate that felsic magmatism lasted for ~10–15 million years (Scheiber et al., 2013;

* Corresponding authors at: School of Earth Science and Mineral Resources, China University of Geosciences, Beijing 100083, China.
E-mail addresses: hui.huang.geo@gmail.com (H. Huang), yaoling.niu@foxmail.com (Y. Niu).

http://dx.doi.org/10.1016/j.lithos.2015.12.018
0024-4937/

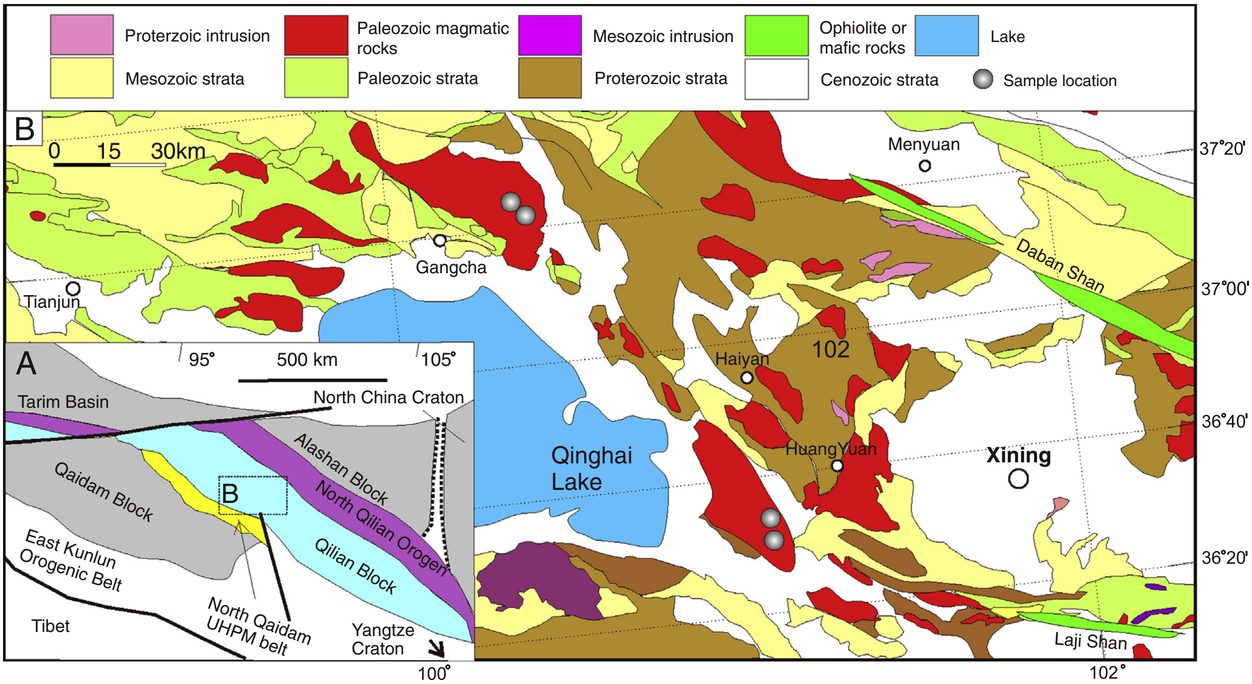

Fig. 1. A, Schematic geological map showing major tectonic units of the Qilian Orogenic Belt (after Song et al., 2013). B, Sample locations in the Gangcha and Huangyuan areas (after Huang et al., 2015 and Pan et al., 2004).

Wang et al., 2013). Based on these information, the large zircon age spread in the granitoids from the QB may indicate a long-lasting magmatism. But the mechanism and tectonic implication is poorly known.

In this study, we focus on a combined geochemical and geochronology study of Huangyuan (HY) and Gangcha (Gcha) batholiths, both of which are in the QB and crop out in excess of ~400 km^2 (Fig. 1B). The new zircon U–Pb ages, zircon Hf isotopes and whole rock Sr–Nd–Pb–Hf isotopes, together with the literature data, enable a revised tectonic model in which long-lasting granitoid magmatism occurred from the onset of the continental collision at ~500 Ma to slab broke off at ~450 Ma, probably related to continued slab steepening.

2. Tectonic setting and geologic background

The QB lies in the middle of the QOB that makes up a broad and composite orogenic belt at the northern margin of the Greater Tibetan Plateau. The QB is bounded by two "suture" zones on its northern and southern boundaries (Fig. 1A, Song et al., 2006, 2013). The terrane to the north is the NQOB consisting of a subduction complex (Song et al., 2013). The terrane to the south is the NQ-UHPM belt, subparallel to the NQOB (Fig. 1A). Yang et al. (2002, 2006) propose that the NQOB and NQ-UHPM are two separate suture zones, whereas Song et al. (2006, 2013) suggest that they are different lithological packages of the same subduction system: the NQOB was the major suture zone with the collision taking place at ~450 Ma. On the other hand, Huang et al. (2015) consider that the collision was located in the NQ-UHPM belt.

The QB had served as a micro-continent during the accretion of the QOB (Huang et al., 2015). The QB has an Archean–Paleoproterozoic crystalline basement (Chen et al., 2007; Li et al., 2007; Huang et al., 2015) with much of it formed in the period of 1.0–0.8 Ga (Guo et al., 1999; Tung et al., 2007a, b; Xu et al., 2007; Song et al., 2012, 2013). The basement consists of granitic gneiss, pelitic gneiss, schist and marble and is overlain by the Palaeozoic sedimentary rocks. The ophiolites exposed at the NQOB–QB boundary have MORB affinity and were dated at 492 Ma (Qinghai Geological Survey Institute, 2006) and 510 Ma (Hou et al., 2005). Palaeozoic I-type and S-type granitoids in the QB have ages of ~446 – 450 Ma and are interpreted as products of seafloor subduction and subsequent continental collision (Yong et al., 2008; Huang et al., 2015). These granitoids are generally coeval with the felsic intrusions within the NQ-UHPM belt (Wu et al., 2001, 2002, 2007, 2011; Gehrels et al., 2003; compilation in Huang et al., 2015). The HY and Gcha plutons are two of the largest plutons in the QB (Fig. 1B). The HY plutonic rocks are typical S-type granites, formed at ~450 Ma (Yong et al., 2008; Huang et al., 2015). The Gcha plutonic rocks are I-type rocks formed at the same time (Huang et al., 2015).

3. Methods

All the analyzed samples were fresh rock chips with weathered surfaces and saw/pen marks removed. All the chips were leached in 5% HCl solution, washed ultrasonically in milli-Q water and dried in a clean environment. Sample descriptions are given in Table 1. Analytical results for samples and standards are given in Tables 2–3, and Tables S1–S4. Major and trace element analysis (Table 2) was done at the Tianjin Institute of Geology and Mineral Resources, China (see Huang et al., 2014). Zircon U–Pb dating (Table S1) was carried out at China University of

Table 1
Sample location and brief description of samples in Qilian Block.

Sample		GPS position		Mineral assemblage	SiO_2%	A/CNK
HY	QL09-04	N36°27.116′	E101°05.634′	Qtz, Kfs, Pl, Bi, Ms	70.0	1.17
	QL09-08	N36°34.895′	E101°13.520′	Bi, Pl, Qtz	67.4	1.06
	QL09-11	N36°46.731′	E101°07.428′	Qtz, Kfs, Pl, Bi, Ms	70.0	1.08
	QL09-13	N36°46.946′	E101°07.603′	Qtz, Kfs, Pl, Bi	72.4	1.04
Gcha	QL10-43	N37°22.629′	E100°28.641′	Bi, Pl, Qtz, Kfs	68.7	1.05
	QL10-36	N37°23.990′	E100°27.498′	Bi, Qtz, Pl, Kfs	72.0	1.14
	QL10-39	N37°23.678′	E100°27.800′	Bi, Qtz, Pl, Kfs	68.4	1.10

Pl: plagioclase; Kfs: K-feldspar; Ms: muscovite; Qtz: quartz; Bi: biotite; HY: Huangyuan; Gcha:Gangcha.
A/CNK = Al/(2 Ca + Na + K).

Table 2
Major and trace elements of granitoids in Qilian Block.

	HY samples				Gcha samples		
	QL09-04	QL09-08	QL09-11	QL09-13	QL10-36	QL10-39	QL10-43
SiO_2	70.0	67.4	70.0	72.4	72.0	68.4	68.7
TiO_2	0.46	0.50	0.23	0.26	0.49	0.61	0.51
Al_2O_3	14.7	16.2	15.8	14.1	13.9	15.1	15.3
Fe_2O_3	0.74	1.06	0.62	0.61	0.82	0.57	0.67
FeO	1.98	2.57	1.06	1.30	2.30	3.57	2.75
FeO_T	2.65	3.52	1.62	1.85	3.04	4.08	3.35
MnO	0.04	0.07	0.04	0.04	0.05	0.05	0.06
MgO	0.95	0.99	0.64	0.73	1.21	1.57	1.38
CaO	1.25	3.08	1.75	1.95	2.46	3.26	2.93
Na_2O	2.34	4.33	3.53	3.17	2.65	3.30	3.29
K_2O	5.90	2.38	5.15	4.37	3.06	2.22	3.54
P_2O_5	0.23	0.22	0.10	0.10	0.11	0.22	0.16
LOI	1.00	0.77	0.82	0.76	0.71	0.65	0.43
Total	98.6	98.8	98.9	99.0	99.1	98.9	99.3
A/CNK	1.17	1.06	1.08	1.04	1.14	1.10	1.05
Li	39.0	89.8	54.5	66.1	56.8	114	49.2
Sc	5.43	7.09	4.36	5.38	9.98	10.4	7.33
Cr	22.7	1.44	8.95	13.2	25.9	29.8	26.6
Co	6.08	3.78	2.54	3.02	6.76	7.84	6.47
Ni	10.6	1.41	2.22	2.42	7.23	7.42	7.64
Ga	21.5	23.9	19.2	18.8	18.6	23.4	19.6
Rb	332	95	179	196	146	162	134
Sr	135	281	292	284	258	249	305
Y	13.9	30.5	15.9	17.2	16.6	25.3	18.5
Zr	249	250	134	131	235	253	210
Nb	20.9	27.7	14.0	17.8	11.0	25.0	14.1
Ba	555	551	969	726	892	273	905
La	63.8	57.0	39.6	28.6	77.6	33.0	53.2
Ce	134	98.9	78.1	48.7	144	61.5	95.9
Pr	16.4	11.5	8.59	5.94	16.6	7.38	11.9
Nd	60.1	39.3	29.8	21.3	58.9	27.5	42.0
Sm	10.5	6.92	5.11	3.86	8.68	5.67	6.82
Eu	0.92	0.99	1.04	0.90	1.42	1.24	1.43
Gd	6.92	6.02	4.07	3.28	6.61	5.39	5.64
Tb	0.81	0.92	0.58	0.53	0.84	0.98	0.76
Dy	3.47	5.38	3.02	3.10	3.88	5.51	3.91
Ho	0.56	1.11	0.59	0.61	0.64	0.96	0.7
Er	1.37	3.07	1.58	1.73	1.6	2.43	1.88
Tm	0.16	0.46	0.23	0.26	0.22	0.34	0.27
Yb	0.84	3.07	1.47	1.76	1.38	2.14	1.73
Lu	0.12	0.46	0.22	0.26	0.21	0.31	0.27
Hf	7.09	6.59	4.09	4.21	6.83	7.64	6.24
Ta	1.22	3.14	1.52	1.81	1.21	1.94	1.20
Pb	42.1	29.1	46.8	42.2	31.9	24.6	27.1
Th	43.0	16.3	19.2	13.5	29.2	13.7	19.5
U	2.81	3.72	1.86	2.57	2.83	2.98	1.41

Geosciences (Wuhan) (CUG, see Liu et al., 2008) and replicated at China University of Geosciences, Beijing (CUGB, see Song et al., 2010). Results from both laboratories are consistent. About 100–150 zircon grains for each of the studied samples were mounted in an epoxy resin disc and then grinded/polished to expose the zircon interiors for imaging and analysis. All the polished zircon grains were photographed under transmitted- and reflected-light, and further examined using CL images prior to U–Pb analysis. Each sample was dated for 30-60 grains. Laser ablation ICP-MS zircon U–Pb analysis was carried on an Agilent 7500 ICP-MS instrument equipped with a GeoLas 2005 at CUG. Each analysis incorporates an approximately 20 s background acquisition (gas blank) followed by 50 s data acquisition from the sample. Detailed operating conditions for the laser ablation system and ICP-MS instrument and data reduction are given in Liu et al. (2008, 2010). The zircon standard 91500 was used as the external standard and ran twice every 5 samples. Rock reference standard GJ-1 were analyzed as unknowns. NIST SRM 610 was used to correct for the time-dependent drift of sensitivity and mass discrimination for trace element analysis. Common Pb was corrected for by ComPbCorr#3_17 (Andersen, 2002). Concordia plots were made using Isoplot (Ludwig, 2003). The results for standard 91500 and GJ-1 are shown in Fig. S2. The obtained mean concordant $^{206}Pb/^{238}U$ ages for 91500 and GJ-1 are 1062.3 ± 1.3 Ma (2σ, n = 202) and 599.7 ± 1.2 Ma (2σ, n = 60), respectively (Fig. S2). These results are consistent with the recommended values (Wiedenbeck et al., 1995; Jackson et al., 2004). Same samples were replicated at CUGB using Agilent 7500a with NewWave SS 193 system. The zircon 91500 was used as the external standard. Standard TEMORA (417 Ma, Black et al., 2003) was analyzed as unknowns. Calibrations for the zircon analyses were carried out using NIST 610 glass as an external standard and Si as internal standard. The obtained mean $^{206}Pb/^{238}U$ ages for 91500 and TEMORA are 1062.5 ± 2.3 Ma (2σ, n = 198) and 417.2 ± 1.7 Ma (2σ, n = 64), respectively (Fig. S2). Isotopic ratios were calculated using GLITTER (ver. 4.4, Macquarie University).

Zircon grains with > 95% U–Pb concordance were analysed for *in situ* Hf isotopes on the same spots (or immediately nearby) as dated for U–Pb ages so as to acquire well-constrained initial Hf isotope ratios. Zircon *in situ* Hf isotopes for the HY samples were analysed using a Nu Plasma HR MC-ICP-MS equipped with a GeoLas 2005 laser-ablation system, with a spot size of 44 μm and a repetition rate of 10 Hz, at the State Key Laboratory of Continental Dynamics, Northwest University in Xi'an, China. The detailed analytical technique is given in Yuan et al. (2008, 2010). Interference of ^{176}Lu on ^{177}Hf was corrected for by measuring the intensity of an interference-free ^{175}Lu isotope and using a recommended $^{176}Lu/^{175}Lu$ ratio of 0.02669 to results of the samples. $^{176}Hf/^{177}Hf$ and $^{176}Lu/^{177}Hf$ ratios of the standard zircon 91500 were 0.282304 ± 0.000004 and 0.00029 (2σ, n = 70). MON-1 and GJ-1 standard zircons were run in the course of analysis and give $^{176}Hf/^{177}Hf$ ratios of 0.282738 ± 0.000002 (2σ, n = 38) and 0.282019 ± 0.000006 (2σ, n = 14) respectively. These results are consistent with the recommended values (Yuan et al., 2008).

The Gcha samples were analyzed using the Neptune multicollector (MC) ICP-MS, equipped with a 193 nm laser, at the Institute of Geology and Geophysics, Chinese Academy of Sciences in Beijing, China (IGG-CAS) following the methods of Wu et al. (2006a, 2006b). The MUD and GJ-1 standard zircons were run during the analysis and give $^{176}Hf/^{177}Hf$ ratios of 0.282500 ± 0.000003 (2σ, n = 66) and 0.282010 ± 0.000004 (2σ, n = 29) respectively. These results are consistent with the recommended values (Yuan et al., 2008, and references therein).

The whole rock Sr–Nd–Pb–Hf isotope compositions (Table 3) were determined on a Thermo Finnigan Neptune Plasma Ionization Multicollector Mass Spectrometer instrument in the Northern Centre at Durham University, UK, with analytical details given in Huang et al. (2014) following Nowell et al. (2003). The international standards NBS987, J&M, NBS981 and JMC475 were used for Sr, Nd, Pb and Hf isotopes, respectively. The long term performance of the Neptune at Durham University for Sr, Nd and Hf isotopes was reported by Nowell et al. (2003). Details relating to standard normalization and precisions are given in Table 3.

4. Results

The petrology of the HY and Gcha samples are described by Huang et al (2015), and only a brief summary is given here. The HY samples (samples with 'QL09' initials, Table 1) are mostly two-mica monzogranite containing quartz, K-feldspar, plagioclase, biotite, ± euhedral muscovite and/or allanite. The Gcha samples (samples with 'QL10' initials, Table 1) are biotite granodiorite, mainly consisting of ± amphibole, biotite, quartz, plagioclase and minor K-feldspar. The Gcha samples are biotite granodiorite without amphibole, but are closely associated with amphibole-bearing granitoids.

4.1. Major and trace elements

The HY samples are felsic (SiO_2, 67.4 – 72.4 wt%) (Table 2) and have high alkalis (Fig. 2F) with A/CNK ratios of 1.05 – 1.18 (Table 2). The Gcha samples are also siliceous (SiO_2: 68.4 – 72.0 wt%) (Table 2). They have lower total alkalis (Fig. 2) but a similar A/CNK ratio of 1.05 – 1.14

Table 3
Whole rock Sr–Nd–Pb–Hf isotopic data. The subscribe refers to the analytical session during which the sample was analysed for isotopic compositions. The averages and reproducibility of multiple measurements of the isotope standards during the appropriate sessions are given below:
1: JMC475, 0.282160 ± 08 (2SD, n = 10); 2: 0.282160 ± 06 (2SD, n = 12). $^{176}Hf/^{177}Hf$ are reported relative to an accepted ratio for JMC475 of 0.282160 (Nowell et al., 1998)
3: J&M, 0.511110 ± 11 (2SD, n = 19); 4: 0.511110 ± 07 (2SD, n = 11). $^{143}Nd/^{144}Nd$ are reported relative to an accepted ratio for J&M of 0.511110 (Thirlwall, 1991)
5: NBS987, 0.710267 ± 10 (2SD, n = 13); 6: 0.710277 ± 15(2SD, n = 9). $^{87}Sr/^{86}Sr$ are reported relative to an accepted $^{87}Sr/^{86}Sr$ ratio for NBS987 of 0.71024 (Thirlwall, 1991)
7: NBS981, $^{206}Pb/^{204}Pb$:16.94102 ± 184;$^{207}Pb/^{204}Pb$:15.49811 ± 142;$^{208}Pb/^{204}Pb$:36.71791 ± 512 (2SD, n = 11)
8: NBS981, $^{206}Pb/^{204}Pb$:16.94083 ± 274;$^{207}Pb/^{204}Pb$:15.49706 ± 115;$^{208}Pb/^{204}Pb$:36.71478 ± 399 (2SD, n = 16).

	HY samples			Gcha samples		
	QL09-04	QL09-08	QL09-13	QL10-36	QL10-39	QL10-43
$^{176}Lu/^{177}Hf$	0.005	0.011	0.01	0.004	0.006	0.006
$^{176}Hf/^{177}Hf$	$0.282209(09)_1$	$0.282617(05)_1$	$0.282526(05)_1$	$0.282400(19)_2$	$0.282510(07)_2$	$0.282505(08)_2$
$_{Hf}(450)$	−11	1.5	−1.5	−4.3	−0.8	−1.1
$^{147}Sm/^{144}Nd$	0.1112	0.1089	0.1156	0.0894	0.1251	0.0985
$^{143}Nd/^{144}Nd$	$0.511806(07)_3$	$0.512191(08)_3$	$0.512177(07)_3$	$0.511992(06)_4$	$0.512096(11)_4$	$0.512102(07)_4$
$_{Nd}(450)$	−11.3	−3.7	−4.3	−6.4	−6.5	−4.8
$^{87}Rb/^{86}Sr$	6.98	0.96	1.95	1.60	1.84	1.24
$^{87}Sr/^{86}Sr$	$0.757360(12)_5$	$0.716540(12)_5$	$0.721497(11)_5$	$0.724951(12)_6$	$0.725992(08)_6$	$0.718970(10)_6$
$I_{Sr}(450)$	0.7126	0.7104	0.709	0.7147	0.7142	0.7116
$^{206}Pb/^{204}Pb$	$18.016(1)_7$	$19.775(2)_7$	$18.997(1)_7$	$18.961(1)_8$	$19.407(1)_8$	$18.848(1)_8$
$^{207}Pb/^{204}Pb$	$15.619(1)_7$	$15.721(1)_7$	$15.678(1)_7$	$15.682(1)_8$	$15.707(1)_8$	$15.672(1)_8$
$^{208}Pb/^{204}Pb$	$39.488(5)_7$	$39.203(5)_7$	$38.659(5)_7$	$40.019(04)_8$	$39.141(04)_8$	$39.352(03)_8$
$^{208}Pb/^{204}Pb_i(450)$	38.04	38.42	38.22	38.73	38.35	38.34
$^{207}Pb/^{204}Pb_i(450)$	15.60	15.69	15.66	15.66	15.68	15.66
$^{206}Pb/^{204}Pb_i(450)$	17.70	19.17	18.68	18.57	18.87	18.62

The $^{147}Sm/^{144}Nd_{CHUR0} = 0.1967$,$^{143}Nd/^{144}Nd_{CHUR0} = 0.512638$, $\lambda(^{87}Rb) = 1.42 \times 10^{-11}\ yr^{-1}$,$\lambda(^{147}Sm) = 6.54 \times 10^{-12}\ yr^{-1}$.
$^{176}Lu/^{177}Hf_{CHUR0} = 0.0332$,$^{176}Hf/^{177}Hf_{CHUR0} = 0.282772$, $\lambda(^{176}Lu) = 1.93 \times 10^{-11}\ yr^{-1}$.
$\varepsilon Hf(t) = [(176Hf/177Hf)sample(t) / (176Hf/177Hf)_{CHUR}(t) - 1] \times 10^4\ (176Hf/177Hf)_{CHUR}(t) = (176Hf/177Hf)_{CHUR0} - (176Lu/177Hf)_{CHUR0} \times (e^{\lambda t} - 1)$

(Table. 2). The Gcha samples exhibit S-type affinity in composition but do not contain characteristic Al-rich minerals (e.g. muscovite, garnet, cordierite etc.). Given their close association with amphibole-bearing diorites in the region (Huang et al., 2015), they are more consistent with being highly evolved I-type granitoids. The chondrite-normalized rare earth element (REE) patterns for the HY and Gcha samples show similar light REE (LREE) enrichment and flat heavy REEs (HREEs) (Fig. 3). The HY sample QL09-04 is exceptional with a clear HREE depletion (Fig. 3) which might have crystallized from a HREE-depleted melt. The HY and Gcha granitoids fall on the trend defined by the previously studied samples and altogether form tight correlations on SiO_2-variation diagrams (Fig. 2).

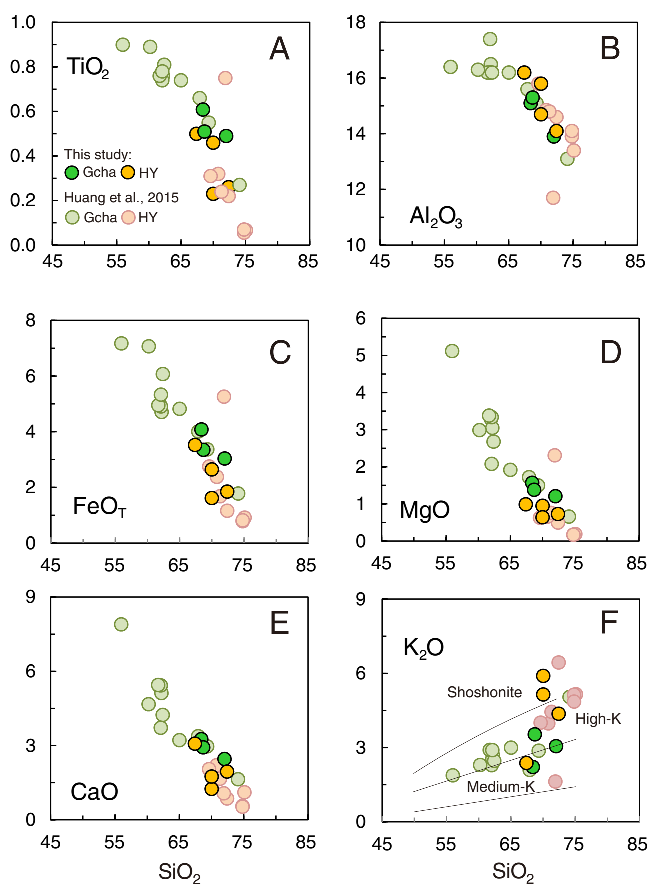

Fig. 2. SiO_2-variation diagrams showing correlated major element compositional variations between samples and sample suites (Gcha—Gangcha; HY—Huangyuan).

4.2. Zircon geochronology

Zircons from the HY samples (except QL09-04) are euhedral, elongated and prismatic with low luminescence and well-developed oscillatory zoning, sector zoning or simply homogeneous (Fig. 4). Igneous zircons have Th/U ratios > 0.2, in contrast with the very low Th/U ratios ≤ 0.01 for metamorphic zircons (Rubatto, 2002; Hoskin, 2003). The Th/U ratios of zircons from HY samples are typically ~0.10 – 1.23 (Table S1), reflecting a magmatic origin. Zircons show uniform within-grain REE composition without clear core–mantle variation (Fig. S1, Table S2).

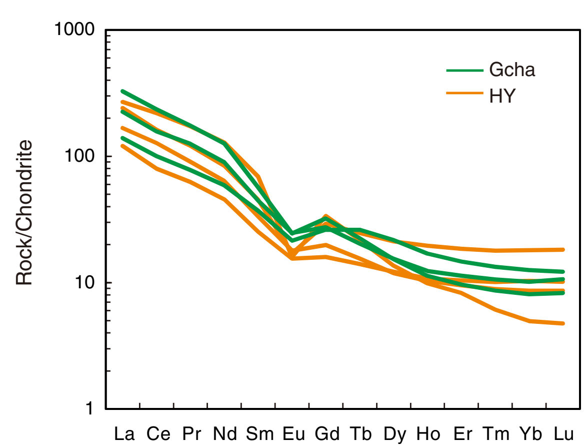

Fig. 3. Chondrite-normalized (Sun and McDonough, 1989) REE patterns for the Huangyuan (HY) and Gangcha (Gcha) samples.

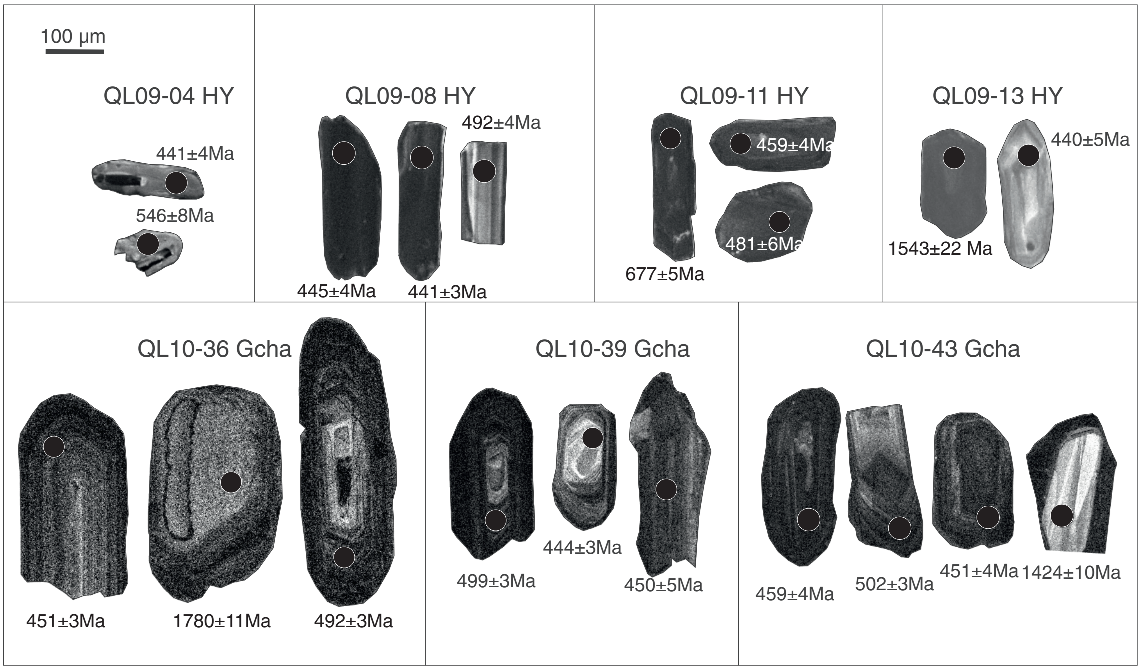

Fig. 4. Cathodoluminescence (CL) images of zircons. White circles black fills are analyzed spots. The numerals are ages in Ma.

The zircon U–Pb ages in each sample range continuously from ~510 – 420 Ma and display a peak at ~445 Ma (Fig. 5). U–Pb ages are not related to compositional variations. The large spread in zircon U–Pb ages is surprising considering the consistent zircon morphology and trace element compositions. Sample QL09-04 with HREE depletion (Fig. 3) shows different CL zircon images and relatively bright luminescence with dark patches (Fig. 4). The zircon U–Pb ages in this sample yield peaks at ~600 and ~445 Ma (Fig. 5). Ages of ~600 Ma are concordant (Fig. 5) and are mostly consistent with being inherited zircons of magmatic origin from a crustal source.

Zircons from the Gcha samples are euhedral and developed good oscillatory zoning. All the analysed spots have Th/U ratios in the range of 0.1 – 1.49 (Table S1). The REE patterns are similar to those of the HY zircons (Fig. S1). Some grains have clear core–rim structure with the core having bright luminescence (Fig. 4). The cores yield concordant or slightly discordant U–Pb ages of 732 – 975 Ma and 1269– 1780 Ma (Fig. 5, Table S1), indicative of their inheritance from the old lithologies. The main zircon populations have continuous U–Pb ages spreading from ~510 to 420 Ma and have major peaks at ~500 Ma and ~450 Ma (Fig. 5).

The continuous age spread from ~420 to 510 Ma (not including the inherited zircons) is obvious in both HY and Gcha samples (Fig. 5). The HY samples have only one peak at ~445 Ma, whereas Gcha samples have peaks at both 500 Ma and 450 Ma. The last panel in Fig. 5 compiles the literature U–Pb ages between 400 Ma and 600 Ma (Huang et al., 2015) including the data of this study. Although SIMS method could provide more precise age data than the LA-ICP-MS method, the observed age spectra are real. Similar age distribution has also been observed (not shown) in many other granitoids and metamorphic rocks, in which the zircon U–Pb data are obtained by the SHRIMP method (Wu et al., 2001; Mattinson et al., 2006; Song et al., 2006; Zhang et al., 2008; Wu et al., 2009).

4.3. Zircon in situ Hf isotopes

Zircon *in situ* Hf isotopes from the HY samples have $_{Hf(450)}$ values varying from −32 to 0 with a peak at −6 and a few more negative values at ~ −50 (Fig. 6A, Table S3), reflecting a rather heterogeneous source. Some inherited Archean zircons in the HY samples have depleted mantle (DM) like initial Hf isotopes (Fig. 6B) indicating juvenile crust growth at ~2.5 Ga. Compared to the HY samples, the Gcha samples have limited $_{Hf(450)}$ variation, dominantly in the range of −6 – 0 with a peak at −2 (Fig. 6A, Table S3). Largely negative $_{Hf(450)}$ values of ~ −30 and ~ −50 are also present, corresponding to those in the HY samples (Fig. 6A). Some inherited Paleoproterozoic zircons in the Gcha samples have DM-like initial Hf isotopes (Fig. 6B, Table S3), indicating juvenile crust growth at ~1.8 Ga.

4.4. Whole rock Sr–Nd–Pb–Hf isotopes

In general, the whole rock Sr–Nd–Pb–Hf isotope compositions are consistent with those of the previous study (Fig. 7, Huang et al., 2015). The HY samples (except QL09-04) have whole rock $_{Nd(450)}$ values that are slightly negative (−4.3 – −3.7), corresponding to the whole rock $_{Hf(450)}$ values of −1.5 – 1.5 (Table 3). Small variations in initial Pb isotopes (Pb_i) ($^{208}Pb/^{204}Pb_i = 38.42–38.04$, $^{207}Pb/^{204}Pb_i = 15.60–15.69$, $^{206}Pb/^{204}Pb_i = 17.70 – 19.17$) and initial Sr isotopic ratios ($I_{Sr(450)} = 0.709$ to 0.713) (Table 3) indicate that contribution from highly enriched upper crust is rather limited. The Gcha samples have whole rock $_{Nd(450)}$ values clustered at −6.4 – −4.8 and $_{Hf(450)}$ values varying from −4.3 to −0.8 (Table 3), generally consistent with zircon Hf isotopes. Pb_i and $I_{Sr(450)}$ overlap with the HY samples (Fig. 7). Sample QL09-04 has $_{Nd(450)}$ and $_{Hf(450)}$ of −11 (Table 3), respectively, indicating significant crustal contribution.

The Gcha and HY granitoids show a large compositional and lithological spectrum with significant correlations between major elements (Fig. 2) and between isotopes (Fig. 7), e.g., significant positive $_{Nd(450)}$- $_{Hf(450)}$ correlation (Fig. 7A). These correlations are best explained as reflecting mixing between the relatively depleted and enriched endmembers, consistent with melting-induced source mixing of varying lithologies (see Niu and Batiza, 1997).

5. Discussion

5.1. The Archean basement of the Qilian Block

The major part of the basement of the Qilian Block has been considered to be Proterozoic on the basis of abundant ~900 Ma granitoids and gneisses. The Palaeo-proterozoic basement age of 2348 – 2470 Ma (Chen et al., 2007; Li et al., 2007) has been largely overlooked. Huang et al. (2015) emphasize the involvement of the Archean Basement in the Paleozoic magmatism. This notion is further supported by the zircon Hf isotope data in this study. The Hf crustal model ages of the zircons (T^{C}_{DM}, calculated by assuming its parental magma derived from continental crust extracted from the depleted mantle following Griffin et al. (2002)) are generally >1.5 Ga (Table S3). This, together with the DM-like $_{Hf(t)}$ values at ca. 1.8 Ga and 2.5 Ga of the older inherited zircons (Fig. 6B), suggests significant continental crust growth within the Qilian Block prior to 1.5 Ga. Zircons with large negative $_{Hf(450)}$ values (up to ~ −50, Fig. 6A) and crustal model ages significantly older than 2.5 Ga (Table S3) require the presence of an Archean basement. In this case, the Qilian Block must have served as a micro-continent during the accretion of the QOB. It is worth to emphasize that the recognition of the presence of an Archean basement of micro-continent origin is significant in the context of understanding tectonic evolution of the region in particular and continental drift/plate tectonics in general because without compositionally depleted and physically buoyant mantle lithosphere of Archean age, the QB would not have its continental drift and amalgamation histories.

5.2. Emplacement age of the HY and Gcha plutons

Huang et al. (2015) pointed out that zircons in both Gcha and HY granitoids from the QB have up to 40 – 60 Myr age span (mostly from 420 to 510 Ma) and thus have poorly constrained crystallization ages. The SHRIMP dating on six zircon grains from the granitoids in the NQ-UHPM belt, south of the QB, also gives a large age range of up to 40 Myr (445–496 Ma) and is interpreted as representing the period from melting to final crystallization in the island arc setting (Wu et al., 2001). Another work on the granites within the NQ-UHPM belt also yields zircon age variation of up to 40 Myrs (~430 – 490 Ma, 10 – 15 analyses for each sample); 'outliers' are excluded and the mean ages define peaks at 465 Ma, 469 Ma and 443 Ma, respectively (Wu et al., 2009). The interpretation of large age spread in the metamorphic rocks has

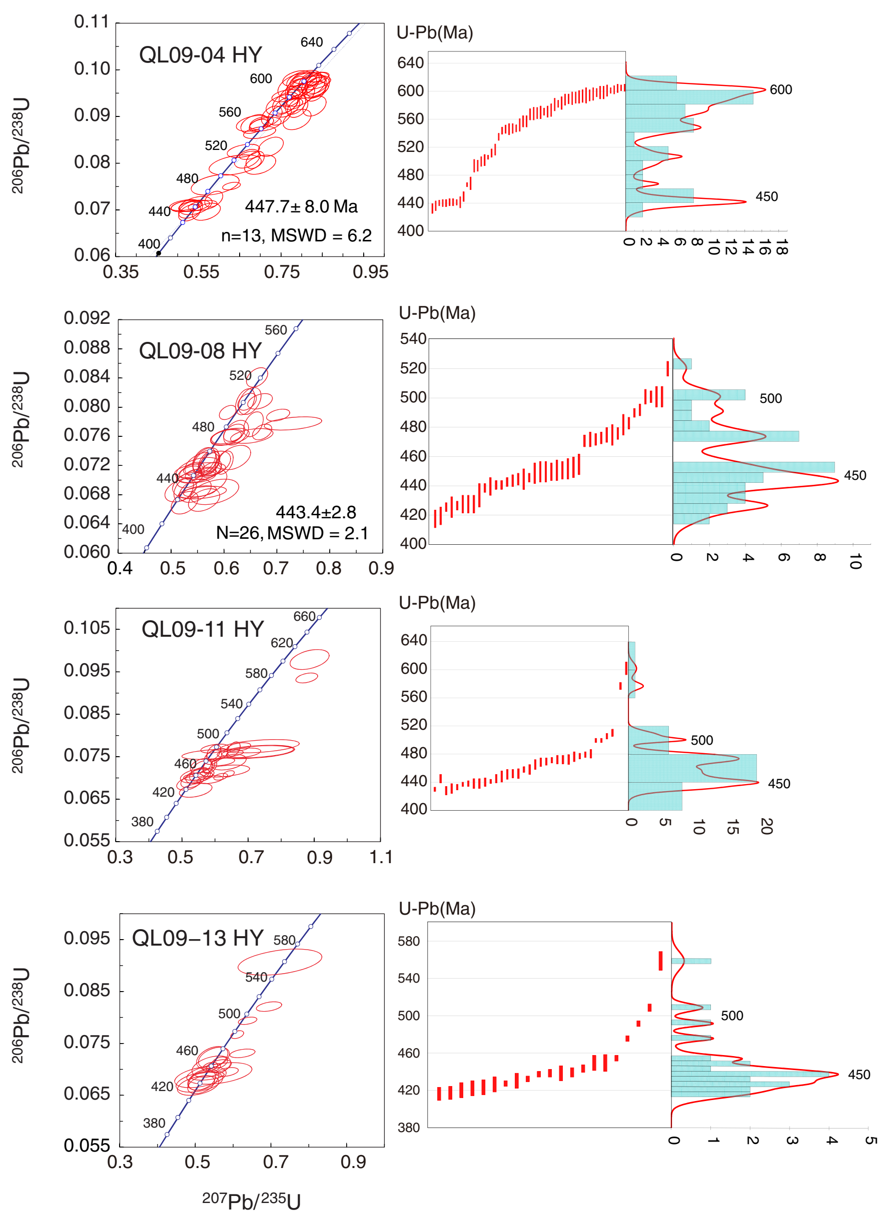

Fig. 5. Zircon U–Pb Concordia diagrams, cumulative probability density plots and histograms for ages (Ma) in each sample. The last two panels summarize the age distributions of the Huangyuan (HY) and Gangcha (Gcha) granitoids, respectively.

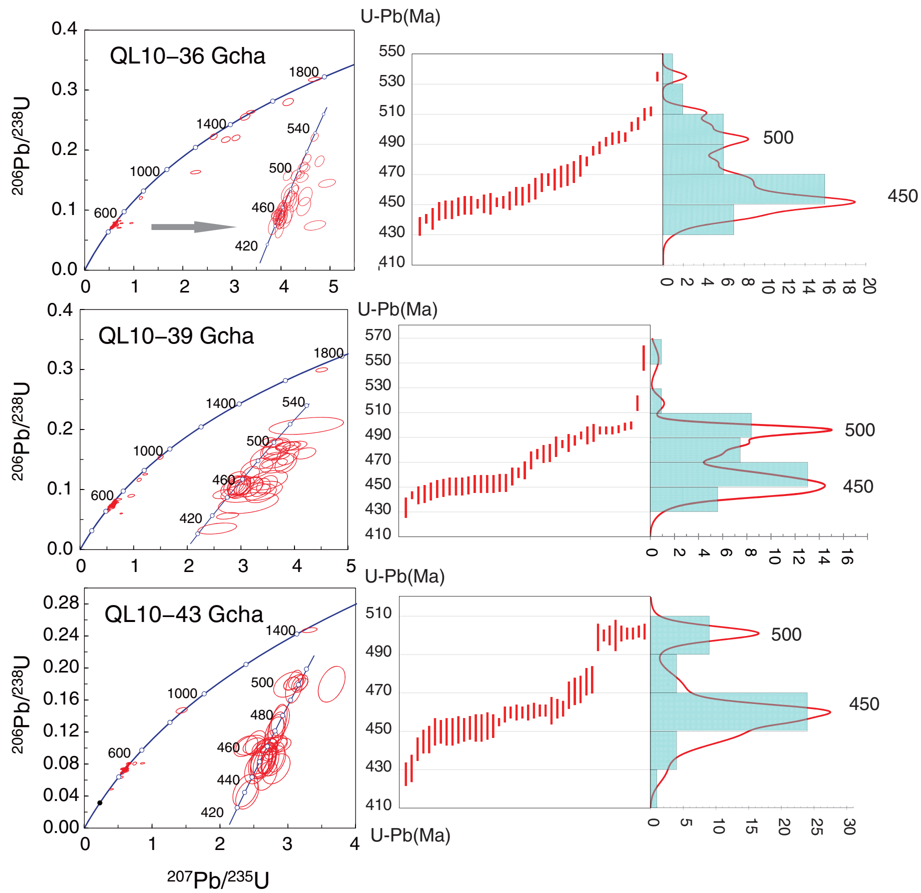

Fig. 5 (*continued*).

been commonly done by grouping zircons according to their contrast in CL-images and compositions. However, for granitoids with such a large age spread, the widely used grouping does not apply because of the absence of such contrast. The possibility of mixing ages could be ruled out because of the lack of the CL image evidence. Minor Pb-loss might be more likely the cause of the spread along the Concordia, as the minor Pb-loss could be easily disguised by the large error ellipses (Scheiber et al. 2013). However, it is unlikely for the distinct granitoids from HY, Gcha and NQ-UHPM to have experienced the same degrees of Pb-loss and thus lead to the same age spectra. The large age spread in the range of approximately 420 – 510 Ma seems to be a common feature for the granitoids in the NQ-UHPM belt and the QB. Some studies have proposed that these granitoids have an emplacement age of ~450 Ma (Wu et al., 2001, 2009; Huang et al., 2015). In this study, we concur with the interpretation that ~450 Ma is the emplacement age due to the significant peak in both the HY and Gcha samples (Fig. 5). However, the peak at ~500 Ma in the Gcha samples (Fig. 5) should also be geologically significant.

5.3. Re-evaluation of previous metamorphic interpretation

Zircons in the eclogites from the NQ-UHPM belt give two major age populations by magmatic cores and metamorphic rims, respectively (Mattinson et al., 2006; 2009; Song et al., 2006, 2013, 2014; Zhang

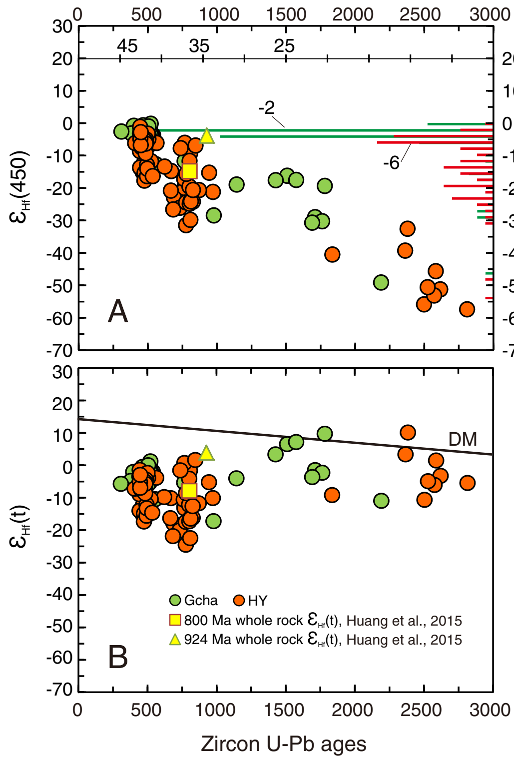

Fig. 6. A, $\varepsilon_{Hf(450)}$ (parts per 10^4 deviation of initial Hf isotope ratios between the zircon sample and the chondritic Hf isotope value at 450 Ma) vs. zircon ages. Hf isotopes are corrected to 450 Ma to show the signatures of source materials involved in the 450 Ma magmatism. Secondary Y-axis: histograms of zircon *in situ* $\varepsilon_{Hf(450)}$ values for the Huangyuan (HY) and Gnagcha (Gcha) granitoids (106 points for the Gcha samples, 77 points for the HY samples). B, $\varepsilon_{Hf(t)}$ vs. the zircon ages. Hf isotopes are corrected to the individual zircon ages to show the isotopic composition of the zircons at the time of crystallization.

et al., 2008). Interpreting U–Pb ages of eclogites requires establishing whether the zircons were inherited from the protolith, formed during subduction metamorphism, or formed during exhumation (Baldwin et al., 2004). The kyanite (ky) eclogites from the Dulan area in the NQ-UHPM assemblage, spatially closest to the granitoids of this study, are of troctolitic (olivine + plagioclase) protolith (Zhang et al., 2008). Magmatic cores of zircons from kyanite eclogites have Th/U values of >0.94 and yield an age of ~516 Ma; metamorphic rims with Th/U ratios of <0.03 are dated at ~445 Ma (Zhang et al., 2008). These two ages were interpreted respectively as the formation age at a mid-ocean ridge and UHP metamorphic age during subduction (Zhang et al., 2008). This interpretation may not be reasonable largely because of very low Zr contents in the bulk rock composition. The basaltic liquids require unrealistically high Zr content (e.g. >5000 ppm) to directly crystallize zircons (Dickinson and Hess, 1982; Hanchar and Watson, 2003; Boehnke et al., 2013). The common interpretation is that zircons found in mafic environments must have crystallized from late stage, evolved melts (Boehnke et al., 2013) or crust-contaminated melts (Zheng et al., 2006). The aforementioned kyanite eclogites possess only 4.63 – 12.15 ppm Zr (Zhang et al., 2008). Although it is difficult to constrain the Zr contents in their parental magmas, it would be arbitrary to simply interpret the ages of magmatic cores as reflecting protolith formation at mid-ocean ridges without additional information because magma parental to kyanite generally only has on average 60 ppm Zr. Zhang et al. (2010) argue this zircon core age as partial resetting age from an 800 Ma basaltic protolith. It is possible that the zircon magmatic cores in the ky-eclogites may have crystallized in other geologic processes (see below).

5.4. Constraints on possible source components

The dominant range of zircon $\varepsilon_{Hf(450)}$ values in the Gcha samples is within −6 – 0 (Fig. 6A), suggesting rather prominent juvenile component in the source for the granitoids. Whereas the scattered zircon Hf isotopes in the HY samples (−50 – 0, mostly −32 – 0, Fig. 6A) point to a rather heterogeneous source with more contributions from the old continental crust. The reworking of the continental crust of Paleoproterozoic to Archean age is evident as manifested by the inherited zircons, large negative zircon ε_{Hf} values and ancient zircon Hf

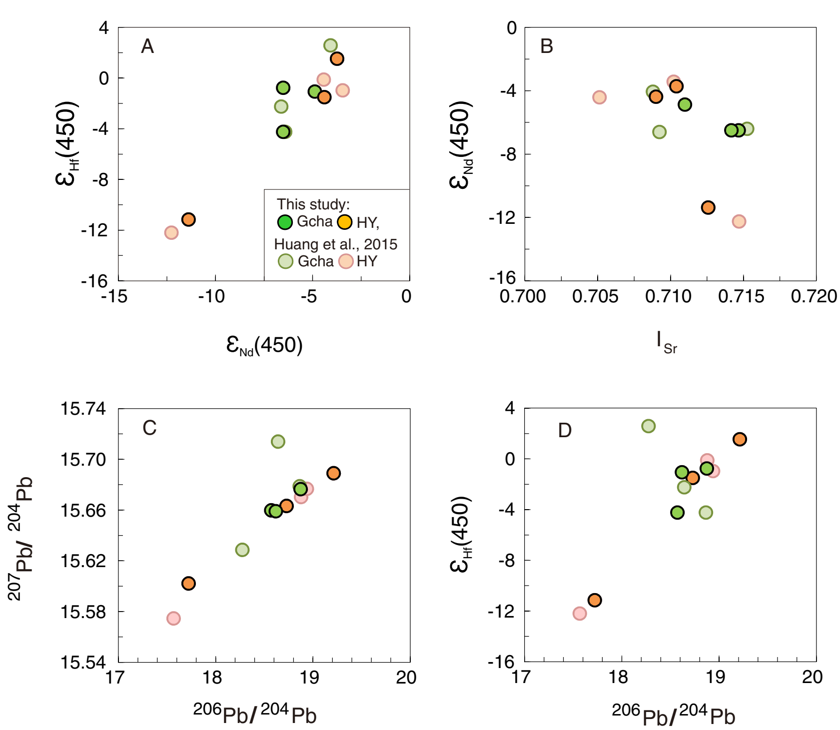

Fig. 7. Isotope plots show that samples in this study have similar isotopic compositions as recently reported (Huang et al., 2015) and have good correlations between isotopes (A–D).

crustal model ages. Some inherited zircon grains possess comparable compositions to the whole rock Hf values of 920 and 800 Ma intrusions, indicating the involvement of the latter lithologies (Fig. 6A, B). Despite these obvious crustal components, the overall small negative whole-rock $_{Hf(450)}$ and $_{Nd(450)}$ values suggest the crustal input either through mixing in the source or through crustal assimilation is actually limited. According to the Nd–Hf isotopic modelling by Huang et al. (2015), the major component in the source is probably the trapped subducting/subducted ocean crust, which can produce andesitic/felsic magmas with significant mantle isotopic signatures. The inevitable fractional crystallization during magma evolution may have contributed to the correlations between the major elements (Fig. 2). The correlations between isotopes, however, point to the importance of mixing between different lithologies. As the two plutons are >150 km apart, the correlated trends are best explained as resulting from varying degrees of melting-induced mixing of varying source lithologies (see Niu and Batiza, 1997), e.g. the subducted oceanic crust, heterogeneous old crustal material and sediments, with superimposed effect of varying extent of fractional crystallization and crustal assimilation.

5.5. Tectonic model and interpretation of U–Pb ages in the granitoids

Understanding the large age range in the HY and Gcha zircons and the temporal and spatial link between QB and adjacent NQ-UHPM belt is important for reconstructing the tectonic history in the region. The granitoids in the NQ-UHPM belt have zircon ages of 420 – 497 Ma (see compilation in Huang et al., 2015), which is coeval with the eclogite-facies metamorphism within the belt (Mattinson et al., 2006; 2009; Song et al., 2006; Zhang et al., 2008). Our granitoids present age range of zircons in individual samples similar to the age spread of zircons within single plutonic samples in the NQ-UHPM belt (see above). Importantly, the age range in zircons from the HY and Gcha plutons overlaps with the age distribution within a single metamorphic rock from the same region (Mattinson et al., 2006; 2009; Song et al., 2006; Zhang et al., 2008). The similarity and close spatial relationship cannot be coincidental but strongly suggest a possibly genetic relationship between the magmatism and metamorphism.

Several studies indicate that the eclogite-facies metamorphism in the NQ-UHPM belt occurred during the period of 460 – 430 Ma (Yang et al., 2002; Song et al., 2003, 2005, 2013, 2014; Mattinson et al., 2006; Xu et al., 2006; Chen et al., 2009a, 2009b; Zhang et al., 2010) and peaked at ~450 Ma (Song et al., 2006, 2014; Zhang et al., 2008). Xu et al. (2006) concluded according to the HPM rocks in the NQ-UHPM that the exhumation started at 470 – 460 Ma. In this case, the collision should have happened perhaps ~20 – 25 Myrs earlier (van Hunen and Allen, 2011), i.e., ~490 Ma, accompanied by intense magmatism (Mo et al., 2008; Niu et al., 2013; Huang et al., 2014). The magmas produced by partial melting of the trapped/subducted upper ocean crust during continental collision are compositionally andesitic to felsic with inherited mantle isotopic signatures (Mo et al., 2008; Niu and O'Hara, 2009; Huang et al., 2014, 2015). The basaltic source required by the whole rock Nd and Hf isotopes modelling for the HY and Gcha samples is probably the trapped subducted/subducting oceanic crust (Huang et al., 2015). The inferred large scale magmatism prior to 470 Ma in the NQ-UHPM belt and the QB has not yet been clearly identified, but the ~500 Ma peak defined by the Gcha samples and the age spread since 510 Ma in both HY and Gcha granitoids as well as in the granitoids within the NQ-UHPM may be evidence for the magmatism initiated during the collision. On the other hand, as aforementioned, the igneous protolith for some eclogites (e.g., the incompatible element depleted troctolite cumulate) were unlikely to have crystallized zircons. There may be alternative interpretations for these magmatic zircon core ages in eclogites. Considering the overlapping ages with the granitoids as well as the overlapping ages between rims and cores of zircons from eclogites in the Qilian Orogenic Belt (Mattinson et al., 2006), we suggest that the magmatic age of ~516 Ma is better explained by zircon recrystallization coeval with the granitoids, during the period of the continental collision; zircon rims grew during later metamorphism.

A close association of the exhumed high-pressure (HP) rocks with contemporary igneous rocks is considered to be indicative of slab break-off (Davies and von Blanckenburg, 1995; von Blanckenburg and Davies, 1995; Sun et al., 2002). Continental collision is not an instantaneous process (Royden, 1993). From the collision to the slab break off, it may take 5 – 40 million years to complete (Gerya et al., 2004; Ghasemi and Talbot, 2006; Andrews and Billen, 2009; Van Hunen and Allen, 2011). Once the collision starts, the subducting oceanic slab steepens further enhanced under gravity. This steepening would open a physical gap which draws a lateral mantle flow (Fig. 8B, Niu, 2005) from the ambient hydrated mantle wedge (Fig. 8B) to form a new asthenospheric mantle wedge in direct contact with the lower crust of the overriding plate where there may be no lithospheric mantle root (Fig. 8A, B).

The newly replenished mantle material may have been partially melted during prior slab subduction and therefore was too refractory

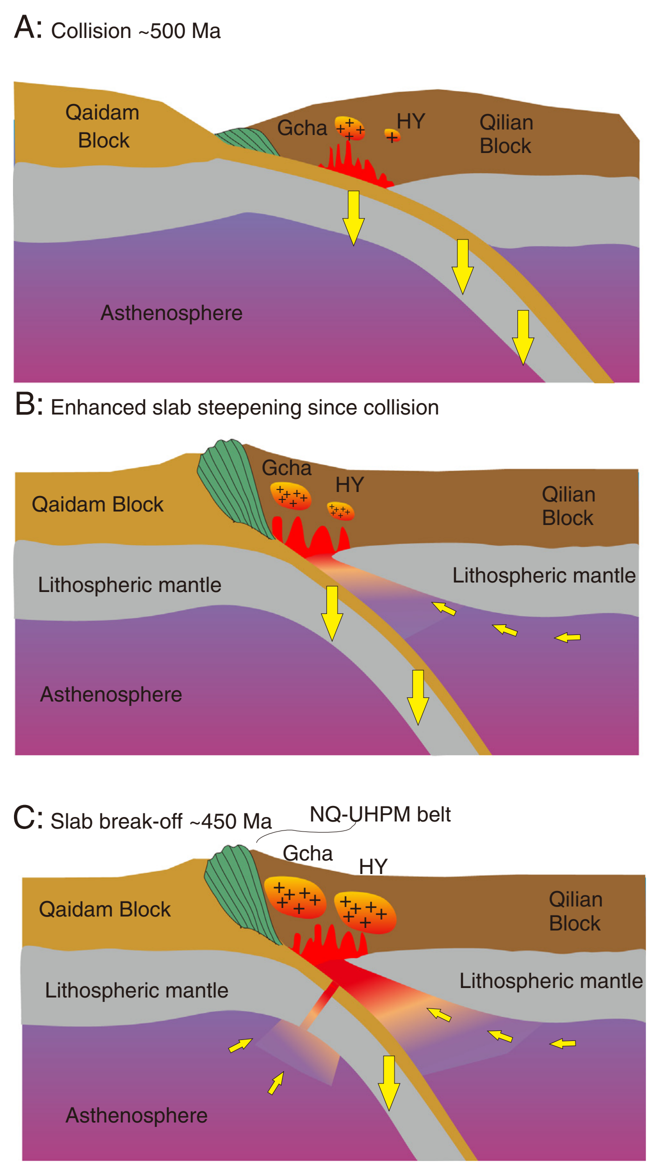

Fig. 8. A, Collision between the Qaidam Block and Qilian Block initiated at ~500 Ma and the syn-collisional magmatism. B, Enhanced slab steepening following collision, induced mantle wedge convection and continuing magmatism. C, ultimate slab break off at ~450 Ma. Big arrow: direction of slab movement; small arrow: mantle flow.

to undergo decompression melting. On the other hand, due to the absence of slab roll-back at this stage, the mantle flow may be sluggish (Kincaid and Griffiths, 2003). Thus, this slow-flowing mantle is easy to turn into the lithospheric mantle due to heat loss, but should still be hot enough to induce partial melting of the lower crust and keep the trapped slab above hydrous solidus (>650 °C, Mo et al., 2008). The trapped/subducted oceanic crust as being the major source for both HY and Gcha granitoids since the onset of collision through slab steepening is consistent with small whole rock $_{\mathrm{Nd}(450)}$ and $_{\mathrm{Hf}(450)}$ values which requires 70 – 80% mantle contribution (Huang et al., 2015). Additional materials from the lower crust and subducted sediments can explain the inherited zircons with large negative zircon $_{\mathrm{Hf}(450)}$ values and wide compositional range. The significant correlations between major elements and between isotopes can be readily explained by melting-induced mixing in a compositionally heterogeneous source (Niu and Batiza, 1997). The dominant age peaks at 450 Ma for both HY and Gcha samples may indicate the extensive heat supply from the convecting asthenosphere due to slab break off (Fig. 8C). It is hard to evaluate if the ages of ~510 – 420 Ma record multiple magma pulses or a continuous long-lasting event based on the analytical precision in this study. Nevertheless, we suggest that partial melting may have continued from onset of the collision at ~500 Ma to the ultimate slab break-off at ~450 Ma, approximately lasting for ~40 – 50 Myrs.

Conclusion

1, The granitoids from the HY and Gcha plutons in the Qilian Block have a large compositional range and define good correlations between major elements and between isotopes. These features are consistent with being products reflecting varying degrees of melting-induced mixing of a compositionally heterogeneous source.

2, The inherited Paleoproterozoic–Archean zircons, the largely negative zircon $_{\mathrm{Hf}(450)}$ as low as to −60 and Archean crustal model ages indicate that the Qilian Block represents an ancient microcontinent. The DM-like Hf isotopes at ~1.8 and ~2.5 Ga point to juvenile crust growth at these times.

3, These granitoids are characterized by a large age spread of ~510 – 420 Ma recorded in zircons with peaks at ~500 Ma and 450 Ma within individual samples, similar to the age distribution in the granitoids and metamorphic rocks in the adjacent NQ-UHPM belt. This feature is best explained by magmatism initiated at the onset of continental collision at ~500 Ma, followed by continued slab steepening until the ultimate slab break-off at ~450 Ma. Magmatic zircon cores in the eclogites dated around ~500 Ma may have actually crystallized during syncollisional magmatism in the context of the continental collision rather than represent the timing of protolith age of ocean ridge magmatism.

Acknowledgement

HH thanks Xiaohong Xia, Pengyuan Guo, Piaoer Fu and Shuo Ding for field accompany, Lei Wu for assistance with trace element analysis and Li Su for help with zircon dating analysis. Discussion with Valentina Magni and Shuijiong Wang was useful. Thanks to Professor Michael Roden and two anonymous reviewers whose comments and suggestions have helped improve this paper significantly. Further thanks are owed to Editor Sun-Lin Chung for editorial effort and constructive comments. The research was supported by Chinese NSFC grants (91014003, 41130314, 41503007) and China Postdoctoral Science Foundation grant (2014M561017).

Appendix A. Supplementary data

Supplementary data to this article can be found online at http://dx.doi.org/10.1016/j.lithos.2015.12.018.

References

Andersen, T., 2002. Correction of common lead in U–Pb analyses that do not report 204Pb. Chemical Geology 192, 59–79.

Andrews, E.R., Billen, M.I., 2009. Rheologic controls on the dynamics of slab detachment. Tectonophysics 464 (1), 60–69.

Baldwin, S.L., Monteleone, B.D., Webb, L.E., Fitzgerald, P.G., Grove, M., Hill, E.J., 2004. Pliocene eclogite exhumation at plate tectonic rates in eastern Papua New Guinea. Nature 431 (7006), 263–267.

Black, L.P., Kamo, S.L., Allen, C.M., Aleinikoff, J.N., Davis, D.W., Korsch, R.J., Foudoulis, C., 2003. TEMORA 1: a new zircon standard for Phanerozoic U–Pb geochronology. Chemical Geology 200 (1), 155–170.

Boehnke, P., Watson, E.B., Trail, D., Harrison, T.M., Schmitt, A.K., 2013. Zircon saturation re-revisited. Chemical Geology 351, 324–334.

Chen, N.S., Wang, X.Y., Zhang, H.F., 2007. Geochemistry and Nd–Sr–Pb isotopic compositions of granitoids from Qaidam and Oulongbuluke micro-blocks, NW China constraints on basement nature and tectonic affinity. Journal of Earth Science 32 (1), 7–21.

Chen, N., Gong, S., Sun, M., Li, X., Xia, X., Wang, Q., Wu, F., Xu, P., 2009a. Precambrian evolution of the Quanji Block, northeastern margin of Tibet: insights from zircon U–Pb and Lu–Hf isotope compositions. Journal of Asian Earth Sciences 35 (3-4), 367–376.

Chen, D., Liu, L., Sun, Y., Liou, J., 2009b. Geochemistry and zircon U–Pb dating and its implications of the Yukahe HP/UHP terrane, the North Qaidam, NW China. Journal of Asian Earth Sciences 35 (3-4), 259–272.

Davies, H.J., von Blanckenburg, F., 1995. Slab breakoff: a model of lithosphere detachment and its test in the magmatism and deformation of collisional orogens. Earth and Planetary Science Letters 129 (1–4), 85–102.

Dickinson Jr., J.E., Hess, P.C., 1982. Zircon saturation in lunar basalts and granites. Earth and Planetary Science Letters 57 (2), 336–344.

Gehrels, G.E., Yin, A., Wang, X.F., 2003. Magmatic history of the northeastern Tibetan Plateau. Journal of Geophysical Research 108 (B9), 2423.

Gehrels, G., et al., 2011. Detrital zircon geochronology of pre-Tertiary strata in the Tibetan–Himalayan orogen. Tectonics 30 (5), TC5016.

Gerya, T.V., Yuen, D.A., Maresch, W.V., 2004. Thermomechanical modelling of slab detachment. Earth and Planetary Science Letters 226, 101–116.

Ghasemi, A., Talbot, C.J., 2006. A new tectonic scenario for the Sanandaj–Sirjan Zone (Iran). Journal of Asian Earth Sciences 26 (6), 683–693.

Griffin, W.L., Wang, X., Jackson, S.E., Pearson, N.J., O'Reilly, S.Y., Xu, X., Zhou, X., 2002. Zircon chemistry and magma mixing, SE China: in-situ analysis of Hf isotopes, Tonglu and Pingtan igneous complexes. Lithos 61 (3), 237–269.

Guo, J.J., Zhao, F.Q., Li, H.K., 1999. Jinningian collisional granite belt in the eastern sector of the central Qilian massif and its implication. Acta Geographica Sinica 20 (1), 10–15 (in Chinese with English abstract).

Hanchar, J.M., Watson, E.B., 2003. Zircon saturation thermometry. Reviews in Mineralogy and Geochemistry 89–112.

Hoskin, P.W.O., 2003. The composition of zircon and igneous and metamorphic petrogenesis. Reviews in Mineralogy and Geochemistry 58, 27–62.

Hou, Q.Y., Zhang, H.f., Zhang, B.r., Zhao, Z.D., Zhu, Y.H., 2005. Characteristics and tectonic affinity of Laji Shan Paleo-Mantle in Qilian orogenic belt:a geochemical study of basalts. Journal of China University of Geosciences 30 (1), 61–70 (in Chinese with English abstract).

Huang, H., et al., 2014. Geochemical constraints on the petrogenesis of granitoids in the East Kunlun Orogenic blet, northern Tibetan Plateau: implications fro the continental crust growth through syncollisional felsic magmatism. Chemical Geology 370, 1–18.

Huang, H., et al., 2015. The nature and history of the Qilian Block in the context of the development of the Greater Tibetan Plateau. Gondwana Research 28, 209–224.

Jackson, S.E., Pearson, N.J., Griffin, W.L., Belousova, E.A., 2004. The application of laser ablation-inductively coupled plasma-mass spectrometry to in situ U–Pb zircon geochronology. Chemical Geology 211, 47–69.

Kincaid, C., Griffiths, R.W., 2003. Laboratory models of the thermal evolution of the mantle during rollback subduction. Nature 425, 58–62.

Li, X.Y., Chen, N.S., Xia, X.P., Sun, M., Xu, P., Wang, Q.Y., Wang, X.Y., 2007. Constraints on the timing of the early-Paleoproterozoic magmatism and crustal evolution of the Oulongbuluke microcontinent: U–Pb and Lu–Hf isotope systematics of zircons from Mohe granite pluton. Acta Petrologica Sinica 23 (2), 513–522 (In Chinese with English abstract).

Liu, Y.S., Hu, Z.C., Gao, S., Gunther, D., Xu, J., Gao, C.G., Chen, H.H., 2008. In situ analysis of major and trace elements of anhydrous minerals by LA-ICP-MS without applying an internal standard. Chemical Geology 257 (1-2), 34–43.

Liu, Y., Gao, S., Hu, Z., Gao, C., Zong, K., Wang, D., 2010. Continental and oceanic crust recycling-induced melt–peridotite interactions in the trans-north China Orogen: U–Pb dating, Hf isotopes and trace elements in Zircons from Mantle Xenoliths. Journal of Petrology 51, 537.

Ludwig, K.R., 2003. A geochronological toolkit for Microsoft Excel. Isoplot 3, 1–70.

Mattinson, C., Wooden, J., Liou, J., Bird, D., Wu, C., 2006. Age and duration of eclogite-facies metamorphism, North Qaidam HP/UHP terrane, Western China. American Journal of Science 306 (9), 683–711.

Mattinson, C., Wooden, J., Zhang, J., Bird, D., 2009. Paragneiss zircon geochronology and trace element geochemistry, North Qaidam HP/UHP terrane, western China. Journal of Asian Earth Sciences 35 (3), 298–309.

Mo, X.X., Niu, Y.L., Dong, G.C., Zhao, Z.D., Hou, Z.Q., Su, Z., Ke, S., 2008. Contribution of syncollisional felsic magmatism to continental crust growth: a case study of the Paleogene Linzizong volcanic Succession in southern Tibet. Chemical Geology 250, 49–67.

Montero, P., Bea, F., Zinger, F., Scarrow, T.F., Molina, J.H., Whitehouse, J.F., 2004. 55 million years of continuous anatexis in Central Iberia: single-zircon dating of the Pena Negra Complex. Journal of the Geological Society 161 (2), 255–263.

Niu, Y.L., 2005. Generation and evolution of basaltic magmas: some basic concepts and a new view on the origin of Mesozoic–Cenozoic basaltic volcanism in eastern China. Geological Journal of China Universities 11 (1), 9–46.

Niu, Y., Batiza, R., 1997. Trace element evidence from seamounts for recycled oceanic crust in the Eastern Pacific mantle. Earth and Planetary Science Letters 148 (3), 471–483.

Niu, Y., O'Hara, M.J., 2009. MORB mantle hosts the missing Eu (Sr, Nb, Ta and Ti) in the continental crust: new perspectives on crustal growth, crust–mantle differentiation and chemical structure of oceanic upper mantle. Lithos 112 (1), 1–17.

Niu, Y., Zhao, Z., Zhu, D.-C., Mo, X., 2013. Continental collision zones are primary sites for net continental crust growth — a testable hypothesis. Earth-Science Reviews 127, 96–110.

Nowell, G.M., Kempton, P.D., Noble, S.R., Fitton, J.G., Sauders, A.D., Mahoney, J.J., Taylor, R.N., 1998. High precision Hf isotope measurements of MORB and OIB by thermal ionisation mass spectrometry: insights into the depleted mantle. Chemical Geology 149, 211–233.

Nowell, G.M., Pearson, D.G., Ottley, C.J., Schweiters, J., Dowall, D., 2003. Long-term performance characteristics of a plasma ionisation multi-collector mass spectrometer (PIMMS): the ThermoFinnigan Neptune. Plasma Source Mass Spectrometry: Applications and Emerging Technologies. Royal Society of Chemistry, Cambridge, pp. 307–320.

Pan, G.T., Ding, J., Yao, D.S.W., L. Q., 2004. Geological Map of the Qinghai–Xizang (Tibet) Plateau and Adjacent Areas. Chengdu Cartographic Publishing House.

Qinghai Geological Survey Institute, 2006. 1:250, 000 regional geological survey digital report of Xining and Menyuan In Chinese.

Royden, L.H., 1993. Evolution of retreating subduction boundaries formed during continental collision. Tectonics 12 (3), 629–638.

Rubatto, D., 2002. Zircon trace element geochemistry: partitioning with garnet and the link between U–Pb ages and metamorphism. Chemical Geology 184, 123–138.

Sawyer, E.W., Cesare, B., Brown, M., 2011. When the continental crust melts. Elements 7, 227–232.

Scheiber, T., Berndt, J., Heredia, B.D., Mezger, K., Pfiffner, O.A., 2013. Episodic and long-lasting Paleozoic felsic magmatism in the pre-Alpine basement of the Suretta nappe (eastern Swiss Alps). International Journal of Earth Sciences 102 (8), 2097–2115.

Song, S.G., Yang, J.S., Liou, J.G., Wu, C.L., Shi, R.D., Xu, Z.Q., 2003. Petrology, geochemistry and isotopic ages of eclogites from the Dulan UHPM Terrane, the North Qaidam, NW China. Lithos 70, 195–211.

Song, S., Zhang, L., Niu, Y., Su, L., Jian, P., Liu, D., 2005. Geochronology of diamond-bearing zircons from garnet peridotite in the North Qaidam UHPM belt, Northern Tibetan Plateau: A record of complex histories from oceanic lithosphere subduction to continental collision. Earth and Planetary Science Letters 234 (1-2), 99–118.

Song, S., Zhang, L., Niu, Y., Su, L., Song, B., Liu, D., 2006. Evolution from oceanic subduction to continental collision: a case study from the Northern Tibetan Plateau based on geochemical and geochronological data. Journal of Petrology 47 (3), 435–455.

Song, S., Niu, Y.L., Wei, C.J., Ji, J.Q., Su, L., 2010. Metamorphism, anatexis, zircon ages and tectonic evolution of the Gongshan Block in the northern Indochina continent—an eastern extension of Lhasa Block. Lithos 120, 3–4.

Song, S., Su, L., Li, X.-h., Niu, Y., Zhang, L., 2012. Grenville-age orogenesis in the Qaidam–Qilian block: the link between South China and Tarim. Precambrian Research 220–221, 9–22.

Song, S., Niu, Y., Su, L., Xia, X., 2013. Tectonics of the North Qilian orogen, NW China. Gondwana Research 23, 1378–1401.

Song, S., Niu, Y.L., Su, L., Zhang, C., Zhang, L.F., 2014. Continental orogenesis from seafloor subduction, continent collision/subduction, to orogen collapse, and orogen recycling: the example of the North Qaidam UHPM belt, NW China. Earth-Science Reviews 129, 59–84.

Sun, S.-S., McDonough, W.F., 1989. Chemical and isotopic systematics of oceanic basalts: implications for mantle composition and processes. Geological Society, London, Special Publications 42, 313–345.

Sun, W.D., Li, S.G., Chen, Y.D., Li, Y.J., 2002. Timing of Synorogenic Granitoids in the South Qinling, Central China: constraints on the Evolution of the Qinling-Dabie Orogenic Belt. The Journal of Geology 110 (4), 457–468.

Thirlwall, M.F., 1991. Long-term reproducibility of multi-collector Sr and Nd isotope ratio analysis. Chemical Geology: Isotope eoscience section 94, 85–104.

Tung, K.A., Yang, H.J., Yang, H.Y., Liu, D.Y., Zhang, J.X., Wan, Y.S., Tseng, C.Y., 2007a. SHRIMP U–Pb geochronology of the detrital zircons from the Longshoushan Group and its tectonic significance. Chinese Science Bulletin 52 (10), 1414–1425.

Tung, K.A., Yang, H.Y., Liu, D., Zhang, J.X., Tseng, C.Y., Wan, Y.S., 2007b. SHRIMP U–Pb geochronology of the zircons from the Precambrian basement of the Qilian Block and its geological significances. Chinese Science Bulletin 52 (19), 2687–2701.

van Hunen, J., Allen, M.B., 2011. Continental collision and slab break-off: a comparison of 3-D numerical models with observations. Earth and Planetary Science Letters 302 (1-2), 27–37.

von Blanckenburg, F., Davies, J.H., 1995. Slab breakoff: a model for syncollisional magmatism and tectonics in the Alps. Tectonics 14 (1), 120–131.

Wang, S.J., Li, S.G., Chen, L.J., He, Y.S., An, S.C., Shen, J., 2013. Geochronolgy and geochemistry of leucosomes in the North Dabie Terrane, East China: implication for post-UHPM crustal melting during exhumation. Contributions to Mineralogy and Petrology 165 (5), 1009–1029.

Wiedenbeck, M., Alle, P., Corfu, F., Griffin, W., Meier, M., Oberli, F., Quadt, A.v., Roddick, J., Spiegel, W., 1995. Three natural zircon standards for U–Th–Pb, Lu–Hf, trace element and REE analyses. Geostandards Newsletter 19, 1–23.

Wu, C.L., Yang, J.S., Ireland, T., Wooden, J.L., Li, H.B., Wan, Y.S., Shi, R.D., 2001. Zircon SHRIMP ages of Aolaoshan granite from the south margin of Qilianshan and its geological significance. Acta Petrologica Sinica 17 (2), 215–221.

Wu, C.L., Yang, J.S., Wooden, J., Liou, J., Li, H., Shi, R., Meng, F., Persing, H., Meibom, A., 2002. Zircon SHRIMP dating of granite from Qaidamshan, NW China. Chinese Science Bulletin 47 (5), 418–422.

Wu, C.L., Yao, S.Z., Zeng, L.S., Chen, S.Y., Li, H.B., Qi, X.X., Joseph, L.W., Mazdab, F.K., 2006a. Double subduction of the Early Paleozoic North Qilian oceanic plate: evidence from granites in the central segment of North Qilian, NW China. Geology in China 33 (6), 1197–1208 (in Chinse with English abstract).

Wu, F.-Y., Yang, Y.-H., Xie, L.-W., Yang, J.-H., Xu, P., 2006b. Hf isotopic compositions of the standard zircons and baddeleyites used in U–Pb geochronology. Chemical Geology 234 (1–2), 105–126.

Wu, C.L., Gao, Y.H., Wu, S., Chen, Q., Wooden, J.L., Mazadab, F.K., Mattinson, C., 2007. Zircon SHRIMP U–Pb dating of granites from the Da Qaidam area in the north margin of Qaidam Basin, NW China. Acta Petrologica Sinica 23 (8), 1861–1875 (in Chinese with English abstract).

Wu, C.L., Wooden, J.L., Robinson, P.T., Gao, Y.H., Wu, S.P., Chen, Q.L., Mazdab, F., Mattison, K., C., 2009. Geochemistry and zircon SHRIMP U–Pb dating of granitoids from the west segment of the North Qaidam. Science in China Series D: Earth Sciences 52 (11), 1771–1790.

Wu, C.L., Xu, X.Y., Gao, Q.M., Li, X.M., Lei, M., Gao, Y.H., Ronald, B.F., Joseph, L.W., 2010. Early Palaezoic granitoid magmatism and tectonic evolution in North Qilian, NW China. Acta Petrologica Sinica 26, 1027–1044 (in Chinese with English abstract).

Wu, C.L., Yao, S.Z., Yang, J.S., Zeng, L.S., Chen, S.Y., Li, H.B., Qi, X.X., 2011. An early Palaeozoic double-subduction model for the North Qilian oceanic plate: evidence from zircon SHRIMP dating of granites. International Geology Review 53 (2), 157–181.

Xiao, W.J., Windley, B.F., Yong, Y., Zhen, Y., Chao, Y., Liu, C.Z., Li, J., 2009. Early Paleozoic to Devonian multiple-accretionary model for the Qilian Shan, NW China. Journal of Asian Earth Sciences 35 (3-4), 323–333.

Xu, Z.Q., Xu, H.F., Zhang, J.X., Li, H.B., Zhu, Z.Z., Qu, J.C., Chen, D.N., Chen, J.L., Yang, K.C., 1994. The Zoulang Nanshan Caledonian subduction complex in the Northern Qilian mountains and its dynamics1. Acta Geologica Sinica-English Edition 7 (3), 225–241.

Xu, Z.Q., Yang, J.S., Wu, C.L., Li, H.B., Zhang, J.X., Qi, X.X., Song, S., Qiu, H.J., 2006. Timing and mechanism of formation and exhumation of the Northern Qaidam ultrahigh-pressure metamorphic belt. Journal of Asian Earth Sciences 28 (2), 160–173.

Xu, W.C., Zhang, H.F., Liu, X.M., 2007. U–Pb zircon dating constraints on formation time of Qilian high-grade metamorphic rock and its tectonic implications. Chinese Science Bulletin 52 (4), 531–538.

Yang, J.S., Xu, Z.Q., Zhang, J.X., Song, S.G., Wu, C.L., Shi, R.D., Li, H.B., Maurice, B., 2002. Early Palaeozoic North Qaidam UHP metamorphic belt on the north-eastern Tibetan plateau and a paired subduction model. Terra Nova 14 (5), 397–404.

Yang, J.S., Wu, C.L., Zhang, J., Shi, R., Meng, F., Wooden, J., Yang, H.-Y., 2006. Protolith of eclogites in the north Qaidam and Altun UHP terrane, NW China: earlier oceanic crust? Journal of Asian Earth Sciences 28 (2), 185–204.

Yin, A., Harrison, T.M., 2000. Geologic evolution of the Himalayan–Tibetan Orogen. Annual Review of Earth and Planetary Sciences 28 (2), 211–280.

Yong, Y., Xiao, W.J., Yuan, C., Yan, Z., Li, J.L., 2008. Geochronology and geochemistry of Paleozoic granitic plutons from the eastern Central Qilian and their tectonic implications. Acta Petrologica Sinica 24 (4), 855–866 (in Chinese with English Abstract).

Yuan, H.L., Gao, S., Dai, M.L., Zong, C.L., Gunther, D., Fontaine, G.H., Liu, X.M., Diwu, C.R., 2008. Simultaneous determinations of U–Pb age, Hf isotopes and trace element compositions of zircon by excimer laser-ablation quadrupole and multiple-collector ICP-MS. Chemical Geology 247 (1), 100–118.

Zhang, G., Song, S., Zhang, L., Niu, Y., 2008. The subducted oceanic crust within continental-type UHP metamorphic belt in the North Qaidam, NW China: evidence from petrology, geochemistry and geochronology. Lithos 104 (1-4), 99–118.

Zhang, J., Mattinson, C., Yu, S., Li, J., Meng, F., 2010. U–Pb zircon geochronology of coesite-bearing eclogites from the southern Dulan area of the North Qaidam UHP terrane, northwestern China: spatially and temporally extensive UHP metamorphism during continental subduction. Journal of Metamorphic Geology 28 (9), 955–978.

Zheng, Y.-F., et al., 2006. Zircon U–Pb age, Hf and O isotope constraints on protolith origin of ultrahigh-pressure eclogite and gneiss in the Dabie orogen. Chemical Geology 231 (1–2), 135–158.